Article:
Depboylu, F.N., Taşkonak, B., Korkusuz, P. et al. (7 more authors) (2024) Cleaning and coating procedures determine biological properties of gyroid porous titanium implants. Emergent Materials, 7. pp. 2711-2729. ISSN 2522-5731

https://doi.org/10.1007/s42247-024-00774-2

Emergent Materials
https://doi.org/10.1007/s42247-024-00774-2

ORIGINAL ARTICLE

Cleaning and coating procedures determine biological properties of gyroid porous titanium implants

Fatma Nur Depboylu[1,2] · Beliz Taşkonak[3] · Petek Korkusuz[4] · Evren Yasa[5] · Olatunji Ajiteru[6] · Kyu Young Choi[6] · Chan Hum Park[7] · Özgür Poyraz[5] · Andrei-Alexandru Popa[1] · Feza Korkusuz[2,8]

Received: 26 March 2024 / Accepted: 18 June 2024

Abstract
Cleaning and coating processes as well as biocompatibility of gyroid commercially pure titanium (Cp-Ti) biomedical implants using the laser powder bed fusion (L-PBF) technology were analyzed. Etching time for cleaning of gyroid Cp-Ti biomedical implants were determined to remove non-melted particles from the surface. Nano hydroxyapatite (nHA) and polylactic acid (PLA) composite coating on the gyroid Cp-Ti implants via dip coating were optimized. Dip coating's withdrawal speed also, the amount of nHA:PLA and viscosity effects of composite were evaluated. 1000 mm/min withdrawal speed prevented clogging of the pores. In addition, silk fibroin was coated on gyroid Cp-Ti implants with electro deposition method. Optimum coating thicknesses were achieved. Biocompatibility after PLA:nHA and silk fibroin were studied. Gyroid and solid Cp-Ti presented 3% and 1% mass loss after a minute of HF/HNO_3 etching. The three-minute etching protocol led to the highest micro pit width formation on the surfaces. 70:30 PLA:nHA and silk fibroin established crack-free coatings on gyroid Cp-Ti surfaces. MTT, live-dead cell assay revealed good biocompatibility after coating.

Keywords Chemical etching · Composite · Silk-fibroin · Dip coating · Electro-deposition technique · Cell viability

1 Introduction

Biomedical metal implants are extensively used for the restoration of the structure and functions of bones and joints [1]. Pores on such implants facilitates the growth of bone cells allowing tissue integration [2]. Commercially pure titanium (Cp-Ti) biomedical implants [3] were recently produced using the laser powder bed fusion (L-PBF) technology and analyzed [3, 4]. Triply periodic minimal surface (TPMS) porous structures based on mathematical modeling of these implants resembled the trabecular bone structure [5]. TPMS such as gyroid was assumed to allow passage of the nutrients, including growth factors through their high permeability among the pores for faster vascularization and bone integration [6]. Producing porous Cp-Ti biomedical implants using L-PBF technology is a

✉ Feza Korkusuz
feza.korkusuz@gmail.com; feza.korkusuz@hacettepe.edu.tr

1 Department of Mechanical and Electrical Engineering (DME) and Mechatronics (Centre for Industrial Mechanics), University of Southern Denmark University, 6400 Sonderborg, Denmark

2 Department of Bioengineering, Institute of Science and Technology, Hacettepe University, Beytepe, Ankara 06800, Türkiye

3 Department of Stem Cell Sciences, Graduate School of Health Sciences, Hacettepe University, 06100 Ankara, Türkiye

4 Faculty of Medicine, Department of Histology and Embryology, Hacettepe University, Atindag, Ankara 06230, Türkiye

5 The University of Sheffield, AMRC North-West, Roy Chadwick Way, Samlesbury Aerospace Enterprise Zone, Mellor Brook, Blackburn BB2 7HP, UK

6 Nano-Bio Regenerative Medical Institute, College of Medicine, Hallym University, Chuncheon 24252, Korea

7 Department of Otorhinolaryngology-Head and Neck Surgery, Hallym University College of Medicine, Chuncheon 24253, Korea

8 Faculty of Medicine, Department of Sports Medicine, Hacettepe University, Altindag, Ankara 06230, Türkiye

Published online: 05 July 2024

novel approach and is therefore less investigated in terms of the cleaning, coating and biocompatibility properties of these structures.

Producing gyroid structures by L-PBF technology may leave non-melted Cp-Ti particles on the surface of the implants [7–9] that may cause particle disease and aseptic loosening. The cleaning process was therefore developed to remove non-melted particles [7] and chemical etching is one of the most widely used methods [10–12]. The commonly preferred acids for etching of Cp-Ti are hydrofluoric acid (HF), nitric acid (HNO_3), hydrochloric acid (HCI), sulfuric acid (H_2SO_4) and acetic acid (CH_3COOH) [8]. The combination of HF and HNO_3 acids was previously recommended in the literature [11]. Hydrofluoric acid releases hydrogen gas due to the reaction with the titanium oxide layer on the surface and this hydrogen gas poses a risk of embrittlement. HNO_3 reacts with the released hydrogen gas, prevents brittleness and passivates it by forming a titanium oxide layer on the surface [13]. The titanium dioxide (TiO_2) formed on the surface ensures that the main material remains bioinert by keeping the water in the biological liquid on the surface, which forms Ti–OH and causes crystallization. The osseointegration feature is also due to the presence of this oxide layer. Bonding the oxide surface with calcium and phosphorus initiates adhesion to the bone [14]. Studies [10, 11, 13] have explored the acid solution ratio and etching time for HF/HNO_3-treated Ti alloys however similar studies for gyroid Cp-Ti biomedical implants were not identified in literature.

Calcium phosphate (CaP) [14] coating of Cp-Ti implants reinforced with polymers is considered as a prefered method to enhance bone ingrowth and tissue integration [15]. The coating processes for Ti biomedical implants with polymer/CaP are well defined [16, 17] in Table 1, however further exploration is needed for L-PBF production of intricate gyroid geometries [18–20]. Coating porous Cp-Ti biomedical implants with poly lactic acid (PLA)-hydroxyapatite (HA) composites was considered to promote the adhesion of osteogenic cells to the surfaces and increase biocompatibility [21], however surface modification process had to be optimized for gyroid structures. Dip coating may provide minimum coating thickness, low operating temperatures and low volume shrinkage for complex porous Cp-Ti biomedical implants [22]. Nonetheless, more research is required to understand the dip coating's immersion duration, deposit, drainage, and evaporation phases for gyroid Cp-Ti biomedical implants [23, 24]. These main parameters of the dip coating process could affect the thickness and the homogeneity of the coating. Silk fibroin is also used for the coating of the Cp-Ti biomedical implants using the electrical deposition technique [25–27] It is a natural protein extracted from *Bombyx mori*, which has been actively used in the field of tissue engineering and regenerative medicine [28]. Dip coating and electrical deposition coating optimizations are generally developed for solid, crack-free and smooth surfaces, obtaining homogeneous 400 nm to 223 µm [16, 17, 28] coating thicknesses. Studies [29] indicated that variations in coating thickness at the implant's edges may result in cracks during

Table 1 Dip-coating parameters of implants

Sample	Coating Comp.	Solution Content	Withdraw. Speed	Cycle	Drying	Thick.	Findings	Ref
Porous Cp-Ti	PLA: nHA	70:30 (PLA:nHA)	1000 mm/min	1	Room temp. 24 hours	400 nm	Homogenous dissolved and no occlusion into the pores.	This study
Ti6Al4V	PLA:HA	0,5 g PLA 0,5 g HA,	510 mm/min.	5	Room Temp. 24 hours	400 nm	Homogeneously coated without any cracks	[16]
Mg	PCL:HA	4%(w/v) ratio PCL % 0, 5, 10, 15 (wt) HA added	-	3	Room Temp. -	50-52 µm	PCL/HA has lower porosity on the surface than HA coating. HA agglomeration is observed	[23]
Ti6Al4V	PCL:HA	PCL (30 wt %) / HA	200 mm/min	5	60°C 12 h at vacuum furnace	223 µm	Thicker and densely coating without any crack	[17]
Iron	PLA:HA	%5 w/v PLA PLA and HA 1:1	200 mm/min	5	Room temp. 48 hours	-	Homogenous dissolved and low agglomeration HA	[24]

PCL Polycaprolactone, *PLA* polylactic acid, *HA* hydroxyapatite

the sintering process. Homogeneous coating of thin-walled gyroid structures that avoid clogging however were not well documented.

In this study, we investigated whether gyroid Cp-Ti biomedical implants could have their cleaning and coating processes improved to achieve desired biocompatibilities, including open porosity and crack-free surface structures. We further asked what the feasibility of the silk fibroin and PLA:HA composite coating materials is on gyroid Cp-Ti discs in terms of biocompatibility. The objective of the study was to develop the cleaning and the coating procedures for gyroid Cp-Ti biomedical implants and to evaluate the biocompatibility of the resulting coating. The effects of the coating materials used on cell viability were therefore evaluated directly and in-directly by in-vitro cytotoxicity tests.

2 Materials and method

We conducted a two-stage controlled cross-sectional study with an inter-disciplinary and multi-center approach. In the first stage, we formulated a cleaning process for gyroid Cp-Ti discs to determine the duration as the dependent variable. In the second stage, we defined the processes for silk-fibroin and PLA:HA coatings. The biocompatibility of these coatings was assessed using the indirect MTT cytotoxicity and the direct live and dead cytotoxicity test.

2.1 Design and manufacturing of the gyroid structures

Gyroid unit cells were designed. They were created in a unit cell size of 3.0 mm and a wall thickness of 0.5 mm. These unit cells were then incorporated into solid discs with a diameter of 6.0 mm and a thickness of 2.0 mm, resulting in the generation of a gyroid disc model using the nTopology (New York, NY, USA) software [30]. Gas-atomized spherical Cp-Ti Grade 2 powder (EOS GmbH Electro Optical Systems, Kralling, Germany) with a particle size (d50) ranging from 38 µm to 45 µm [31] was utilized in the EOS M290 L-PBF device by using the EOSPRINT 2.8 software (EOS GmbH Electro Optical Systems, Kralling, Germany) to produce the gyroid Cp-Ti discs. The resulting gyroid Cp-Ti discs exhibited full density and high dimensional accuracy [4] (Table 2).

2.2 Cleaning process

Gyroid Cp-Ti discs were chemically etched with HF (70%) (Merck, USA) and HNO_3 (65%) (Chemlab, Belgium) acidic solution for one, two and three minutes and shown in Fig. 1. Solid and un-etched Cp-Ti discs established the control group. There were 24 samples for the studies, three gyroid disc samples and three solid disc samples in control group, one, two and three minutes etching groups. Remaining particles on the sandblasted gyroid discs were ultrasonically washed using a mixture of aminoethanol polyethylene glycol (HT1170, Deconex, Netherlands) and potassium hydroxide (HT1401, Deconex, Netherlands) diluted in distilled water. The discs were then de-acidified in distilled water for ten minutes and dried at room temperature. This process was repeated after chemical etching.

Table 2 Optimized L-PBF process parameters

Laser Power (W)	Scan Speed (mm/s)	Hatch Distance (µm)	Layer Thickness (µm)	Volumetric Energy Density (J/mm^3)
150	1500	100	60	16.67

2.3 Coating process of Cp-Ti discs

2.3.1 Dip coating process with PLA:nHA composite

PLA (L210 Evonik, Germany) was initially mixed with chloroform and dissolved in a magnetic stirrer at 40 °C and 300 rpm for six hours and shown in Fig. 2. Nano-sized hydroxyapatite (Nanografi, Turkey) was subsequently incorporated into the PLA solution and stirring was continued for an additional four hours with 500 rpm at room temperature. Gyroid Cp-Ti discs were immersed in the PLA:nHA solution using a dip-coating instrument (KSV Nima Dip Coater, Biolin Scientific, Stockholm, Sweden). The amount of nHA to prevent crack propagation, the quantity of chloroform to control the solution's viscosity and withdrawal speed were adjusted during the coating optimization and shown in Table 3.

Effects of nHA Amount on Crack Propagation and Coating Homogeneity of Solid Cp-Ti Discs Two distinct sol–gel composite solutions were prepared to investigate the effects of the amount of nHA on coating deposition and crack formation. In the first solution, 0.5 g of nHA was added to 0.5 g of PLA, which was dissolved in 30 ml of chloroform resulting in a PLA:nHA ratio of 50:50 in the elution. For the second solution, the same amount of PLA was dissolved in chloroform. This time 0.21 g of nHA was added, which led to a PLA:nHA ratio of 70:30. The solid Cp-Ti discs were then coated with each of these solutions by a single dipping process, employing a withdrawal speed of 300 mm/min. Coated discs were left to dry overnight at room temperature subsequently. This experimental setup was devised to examine the impact of nHA content on the coating process and the formation of cracks in the resulting composite materials.

Withdrawal Speed and Viscosity Effects on Gyroid Cp-Ti Discs Gyroid discs were then subjected to a dipping process at withdrawal speeds of 300, 500, 750 and 1000 mm/min.

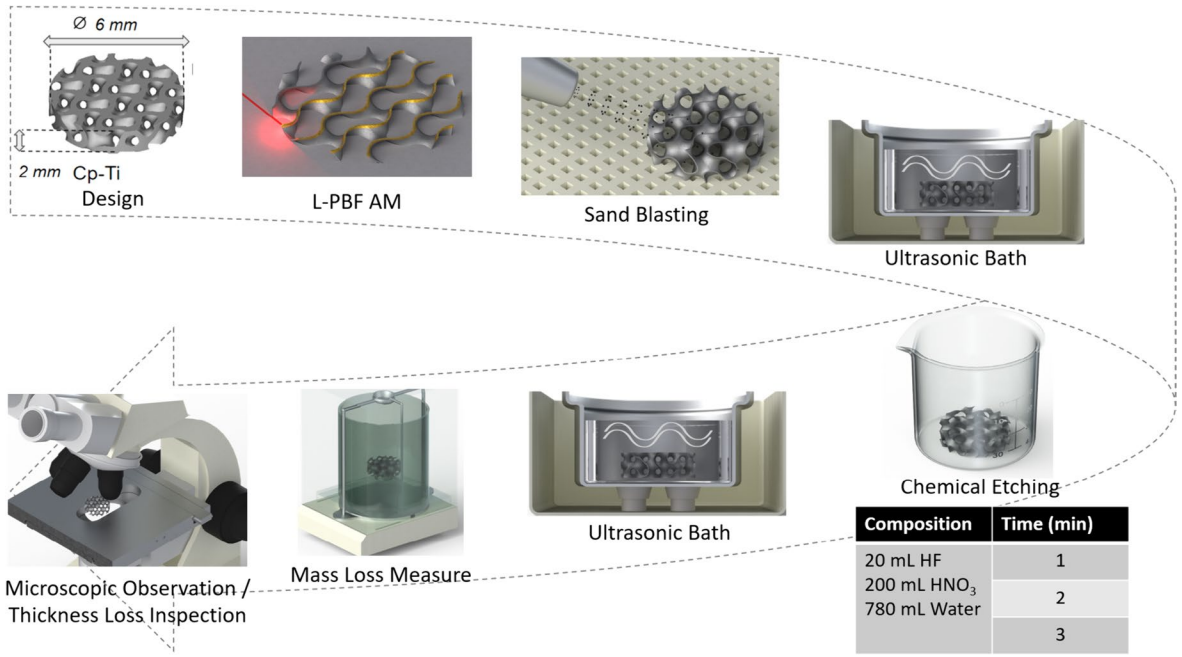

Fig. 1 Steps of the cleaning processing

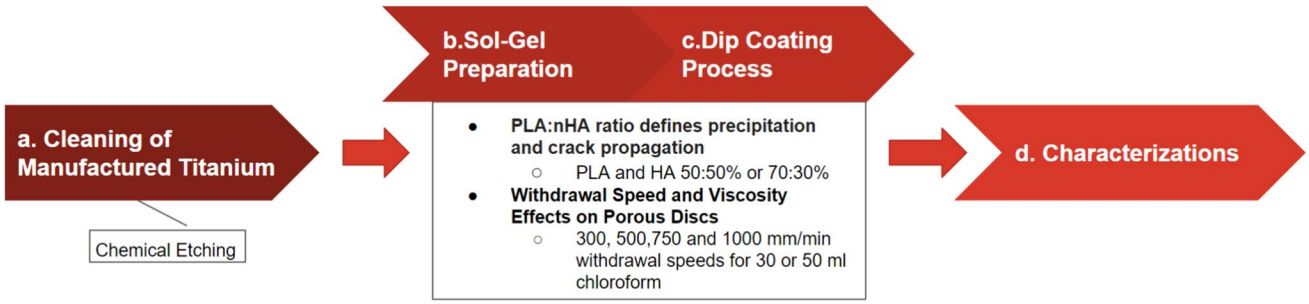

Fig. 2 The coating processes

Table 3 Test plan of PLA:nHA composite coating process

Processes	Characterizations	Cp-Ti Disc	PLA:nHA (%)	Withdrawal Speed (mm/min)	Amount of Chloroform (ml)
Coating Process Optimization	Crack Propagation	Solid	50:50 70:30	300	30
	Viscosity Effect	Porous	70:30	300 500 750 1000	30 50
	Coating Thickness	Solid	70:30	300 500 750 1000	50
Biocompatibility Test Samples	Cell Viability	Porous	50:50 70:30	1000	50

The elution's chloroform content was increased from 30 to 50 ml to further explore the impact of viscosity. A second elution was prepared. The coating process using the second elution was conducted at the same withdrawal speeds (300, 500, 750 and 1000 mm/min) as in the first step and shown in Table 3. The coated discs were dried at room temperature afterwards.

2.3.2 Electro deposition coating with silk fibroin

Silk fibroin (SF) protein was obtained by firstly degumming *B. mori* silkworm cocoon and then rinsing and drying as described previously [32]. 2% and 5% concentrations of SF solution were attained by adding 0.2 g and 0.5 g of SF to 10 ml of phosphate buffered saline (PBS), respectively. The Cp-Ti samples were first washed in an ultrasonic bath with 70% ethanol and then the electrocoating process was initiated as shown in Fig. 3. A platinum wire was connected to the cathode of a 20 V power supply, while Cp-Ti was connected to the anode electrode of the same power supply at a distance of one centimeter in the collection cup containing the SF solution. The power was switched on for 60 s, which resulted in uniform deposition of SF on the surface of the Cp-Ti. Coating was repeated with the newly formed 2% SF and 5% SF solutions. Coatings were fixed with 80% methanol for five minutes afterwards, frozen for a day and dried for three days at room temperature.

2.4 Characterizations

2.4.1 Cleaning characterizations

Sample images were obtained using a stereomicroscope (MZ16A Leica, Germany) and a scanning electron microscope (SEM) (FEI Nova NanoSEM, the Netherlands) to observe the formation of micro-pits on the surfaces. The mass loss of each sample was measured on a precision balance (AXIS ALN 220G, Poland). Wall thicknesses were measured using a stereomicroscope (MZ16A Leica, Germany) for assessing the dimensional accuracy of thin walls between the designed and produced parts.

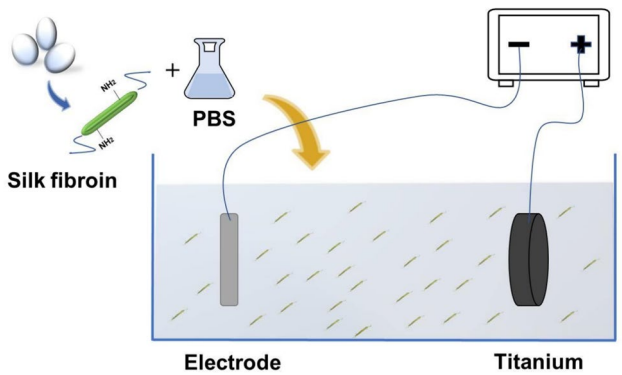

Fig. 3 SF Coating process with electrodeposition method

2.4.2 Coating characterizations

Surface Characterization of Coating Surface analysis of the solid and the gyroid Cp-Ti discs were performed with a SEM (FEI Nova NanoSEM, the Netherlands) for characterization of the PLA:nHA composite coating. Energy dispersive X-ray spectroscopy (EDS) was applied to quantify the chemical deposition of the coating. A SEM (Carl Zeiss, Germany) and fluorescence microscope (Eclipse 80i, Nikon Instruments Inc., USA) were used for the surface characterization of the silk-fibroin coating.

Coating Thickness Measurement The discs were prepared in 500 and 1000 grids, then polished with colloidal silica (Struers, Denmark) solution to obtain a mirror surface finish during the first stage of the process. They were cleaned by ultrasonic washing with ethanol for fifteen minutes afterwards. Surface profilometry (Dektak, Brukel) was used for measuring the coating thickness. Half of the solid Cp-Ti disc surface was covered by masking method, and the other half of the surface was left uncoated as a reference for coating thickness benchmark. The needle tip of the profilometer was then moved along the surface towards the coating to obtain the necessary measurements.

Biocompatibility Cytotoxicity Analysis by MTT The MTT cytotoxicity test, following the ISO 10993–5 standard, was used to analyze the biocompatibility of the gyroid Cp-Ti discs. The commercially available L929 cell line (CCL-1, ATCC, USA) was used. 10^5/ml cells were cultured in a solution containing DMEM (Dulbecco's Modified Eagle's Medium), 10% FBS (Fetal Bovine Serum), 1% Pen-Strep (Penicillin–Streptomycin) and 1% L-glutamine of culture medium in each well of a 96-well plate (Sarsted, Germany). Cells were then incubated in a 5% CO_2 environment at 37℃ for 22 to 26 h. Proliferating cells attached to the culture flask in their second passage and exhibited their typical needle-like appearance. A 100 µl extract-containing solution was added to the wells and incubated for four hours. The solution was entirely removed from the wells after analyzing cell growth and attachment under a light microscope. 50 µl of the MTT solution was then added and incubated for two hours. Following this, 100 µl of isopropanol was added to each well. The wells were then transferred to a microwell reader and cell viability analysis was conducted at a wavelength of 570 after purging the MTT solution. The uncoated gyroid Cp-Ti discs, the coated gyroid Cp-Ti discs 1 (70:30 PLA:nHA), the coated gyroid Cp-Ti discs 2 (50:50 PLA:nHA), the polyethylene (negative control), the latex (positive control) established the experimental and control

groups as shown in Table 4. The tests were carried out with a total of 20 samples using four samples in each group. All groups were sterilized with ethylene oxide before the cytotoxicity test. Samples were kept in 500 µl medium per sample for 24 h at 37 °C in order to obtain extracts from the materials. Extracts were added to the wells when the seeded cells reached 70% of confluency. At the end of 12, 24 and 48 h, the medium was replaced with 100 µl of fresh medium and 10 µl of MTT solution was added. The samples and the cells were then incubated for 4 h at 37 °C in a humidified environment with 5% CO2. 50 µl of DMSO was added to 25 µl of medium that was left in each well in order to dissolve the formed formazan crystals. After waiting for ten minutes, absorbance values were recorded in a microplate reader (VersaMax) at a wavelength of 570 nm.

Cell Viability Analysis by Live and Dead Cell Assay Primary human dermal fibroblasts (HDF, PCS-201–012) were purchased from the American Type Cell Collection and passaged once they reached 80% confluence. The media was supplemented with %15 heat inactivated fetal bovine serum (FBS) along with 100 U/mL penicillin and %1 L-glutamine. Cells were seeded in 48 well plates at 1×105 /ml and incubated for 24 h. To sterilize, samples were exposed to UV light on both sides for five minutes. A cell suspension was prepared through centrifugation and then carefully added to each sample using the dropwise method, with a volume of 50 µl. After an hour of incubation for cell attachment, the medium was removed and the L&D solution was prepared according to kit instructions. A mixture was prepared by combining 6 ml of cell culture medium with 6 ml of PBS in a 1:1 ratio. 5 µl of Calcein AM (Merck KGaA, Darmstadt, Germany), 20 µl of Propidium iodide (Merck KGaA, Darmstadt, Germany) and 8 µl of Hoechst 33342 (Merck KGaA, Darmstadt, Germany) were added to the mixture to create a 12 ml dye solution. Red dye (Propidium Iodide) binds only to DNA, it can pass through the damaged cell membrane and indicates dead cells, whereas green dye (Calcein AM) stains DNA, protein, cellular organelles of living cells because it is hydrolyzed by intracellular enzymes. Blue dye (Hoechst) stains the cell nucleus, so it aims to identify cell morphology. The components were thoroughly mixed by vortexing the dye solution. Appropriate volume of the dye mixture was added to each well, incubated for one hour at 37°C. After incubation, dye solution was suspended, and cells were fixed with 4% paraformaldehyde. Confocal microscopy (LSM 980, Zeiss, Germany) was carried out on days 1, 3, 5 and 7 by producing 26 z stacks per each sample. Z stacks have been quantitatively analyzed using 3D Tool Kit (Zen Lite 3.8, Oberkochen, Germany) for 3D cell segmentation as determined in Table 4. Briefly, live green–blue, dead red-blue and the total cell volumes were quantified for each sample. Then, the live and dead cell volume to total cell volume ratios were calculated. The same test protocol was also followed on the cell viability of silk fibroin. The live and dead images (live cells stained green with calcein-AM and dead cells stained red with Ethidium homodimer), recorded by confocal microscopy (K1-Fluo, Nanoscope Systems Inc., Korea), show that HDF cells proliferated well in all groups (Cp-Ti without silk fibroin coating, Cp-Ti with 2% silk fibroin coating, and Cp-Ti with 5% silk fibroin coating) until day seven of cultivation.

Statistical analysis The Kruskal–Wallis test and the Mann–Whitney test with Bonferroni correction and multiple comparisons between groups were undertaken for the data set which was determined to be non-parametric after evaluating the normal distribution with the Shapiro–Wilk test. A 95% confidence interval was set and descriptive statistics were presented with minimum, maximum and median graphs.

Table 4 Biocompatibility analysis workflow

MTT	Groups	n	Analysis hours			
			12th	24th	48th	
	Uncoated Cp-Ti	4	Microwell reader			
	Coated 1 (70:30 PLA:nHA)	4				
	Coated 2 (50:50 PLA:nHA)	4				
	Polyethylene (Negative C.)	4				
	Latex Glove (Positive C.)	4				
L&D Assay Kit	Groups	n	Analysis days			
			1st	3rd	5th	7th
	Uncoated Cp-Ti	1	Confocal & SEM			
	Coated 1 (70:30 PLA:nHA)	1				
	Coated 2 (50:50 PLA:nHA)	1				
	Uncoated Cp-Ti	1				
	2% SF	1	Confocal			
	5% SF	1				

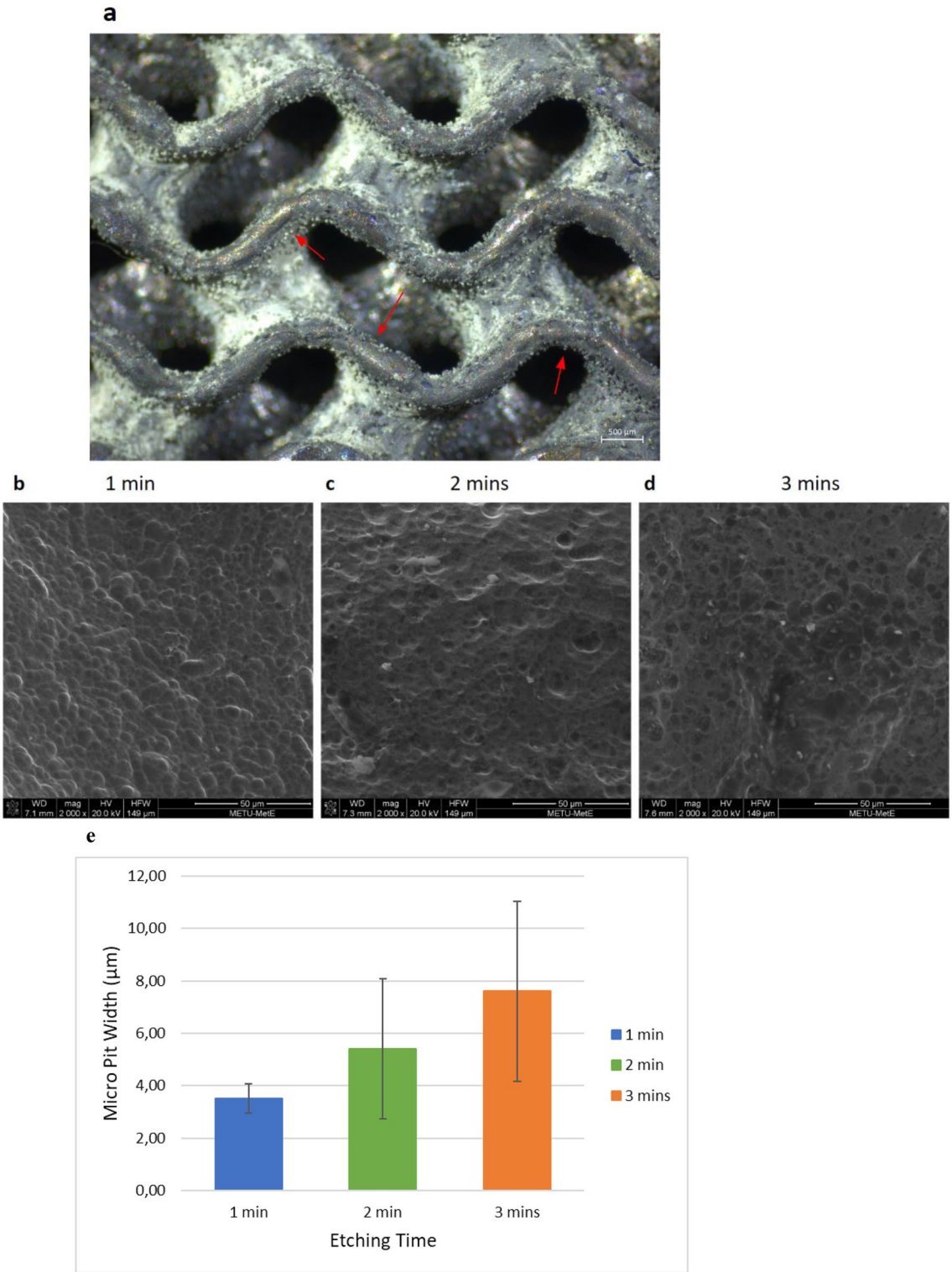

Fig. 4 LOM and SEM images of the non-etched (**a**), one (**b**), two (**c**) and three (**d**) minutes etched thin wall surfaces of gyroid Cp-Ti discs. Average width of micro pits in one, two and three minutes (**e**)

3 Results and discussion

3.1 Cleaning process results and discussions

Surface characterizations of cleaning process Non-melted particles, which adhered to the non-etched surfaces as shown in Fig. 4(a) were successfully removed in all groups. In accordance with DIN ISO 1332, non-melted particle size was determined by laser diffraction to be between 38 and 45 µm [31]. Micro pits formation was another determinant of the cleaning process even though removal of the non-melted particles was achieved. Two studies [8, 9] proved that micro pits may cause mechanical strength loss. In contrast, one of these studies [9] demonstrated that 5 µm micro pits have advantages for the coating adhesion to the tissue surface. They increased stability and supported rapid osseointegration into the bone. Micro pits formed and distributed homogeneously on the one, two- and three-minutes etching groups in this study as shown in Fig. 4(b), (c) and (d). The pits gradually widened and deepened as time increased. The micro pit width of the one-minute group was approximately 3,5 µm while the two and the three minutes groups presented approximately 5,5 µm and 7,5 µm widths as shown in Fig. 4(e). A previous study [8] stated that the micro pits were beneficial to provide controlled surface roughness for different applications. As a result, the micro pits obtained in a minute in our study were in line with the literature, with a width size that should cause minimal mechanical loss and provide high bone integration.

Mass loss The three minutes etching process resulted in the greatest mass loss for both gyroid and solid Cp-Ti discs. The gyroid discs exhibited approximately 5% higher mass loss,

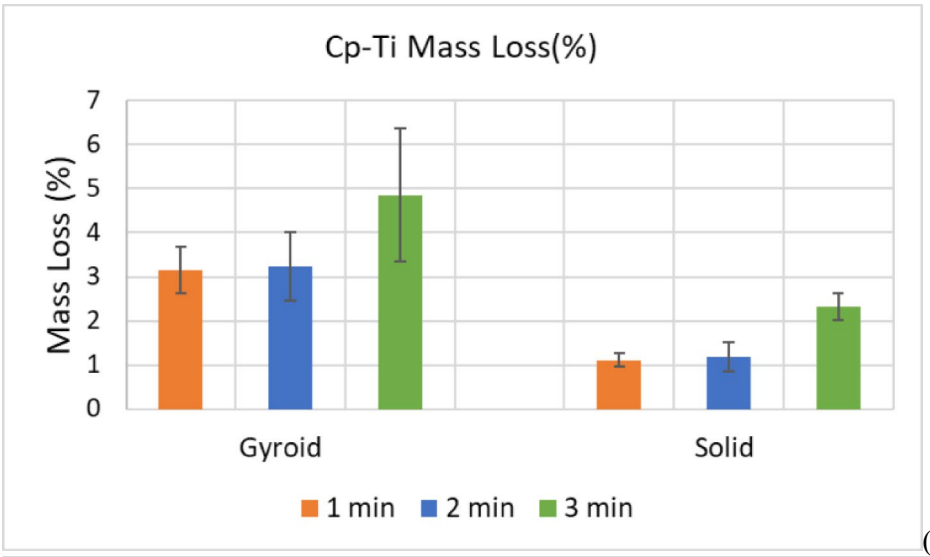

(a)

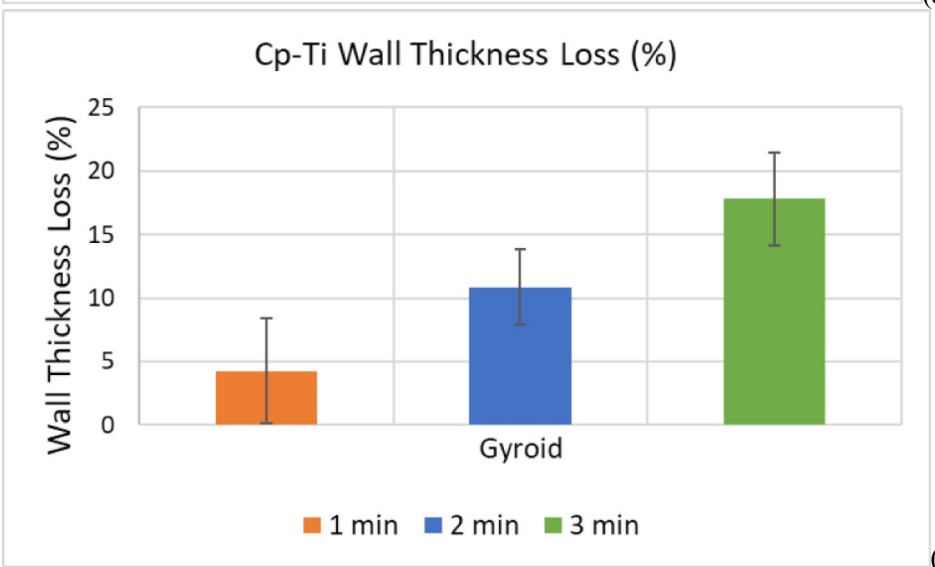

(b)

Fig. 5 **a** Mass loss in gyroid and solid samples as a result of one, two and three minutes of chemical etching of Cp-Ti discs, (**b**) Wall thickness losses as a result of one, two and three minutes of chemical etching in gyroid Cp-Ti discs

which can be attributed to their larger surface area, while the solid ones presented a mass loss of 2.3%. In the one- and two-minutes groups, the gyroid discs presented a mass loss of more than 3%, whereas the solid discs had a loss of 1.1% as shown in Fig. 5(a). The minimum mass loss was calculated to be in the one-minute etching group in our study. This time was selected due to aiming for minimum mechanical loss even if the mechanical tests were not applied to the etched Cp-Ti discs. The reason was that the mass loss and the mechanical yield strength loss were correlated [7].

Gyroid wall thickness loss The highest gyroid Cp-Ti wall thickness loss occurred after three minutes of etching, with a reduction of 18%. The thickness loss was 11% at two minutes while it was 4% at a minute and shown in Fig. 5(b). The results for wall thickness were in line with the conclusions of a previous study [10] which reported a 17% decrease after three minutes of etching using the same acidic composition. A different study [8] revealed a 13% reduction in wall thickness through the use of chemical etching. The cleaning process time optimization provided an advantage to control mechanical properties. Thickness loss calculations could be a good frame for optimizing wall thicknesses that can tolerate this loss. The three minutes chemical etching process consequently led to a significant micro-pit formation on the surface along with a high mass and wall thickness loss in this study. The mass loss in the one-minute and two-minute etching groups was comparable. The initial stages of the chemical process might show the similarity due to the powder metallurgy and dealloying processes. The chemical solvent can lead to remove the certain elements from the titanium [33]. Our experiments therefore proceed with the one-minute etching group as it resulted in the least mass loss and thickness reduction. The optimum etching time of a minute created a suitable ground in terms of both adhesion of the coating to the surface and a minimum mechanical loss during the cleaning process.

3.2 Coating process results and discussions

3.2.1 PLA:nHA composite coating

The amount of nHA effect on coating accumulation and crack propagation Macroscopical observation presented that 50:50 PLA:nHA resulted in a higher precipitation on the surface compared to 70:30 PLA:nHA as shown in Fig. 6. This caused the formation of higher cracks in the coating. The crack and nHA deposition were formed at the edge of the disc due to gravity. SEM images in Fig. 6 captured from the coating transition zones revealed that the distribution of nHA on PLA was uniform in both coatings regardless of the nHA amount that was used. Crack propagation was not observed during the transition of the surfaces of the two Cp-Ti discs although the edge of the 50:50 PLA:nHA one presented a crack. Two studies [16, 24] applied 50:50 PLA:HA as determined in Table 1. The coating thicknesses

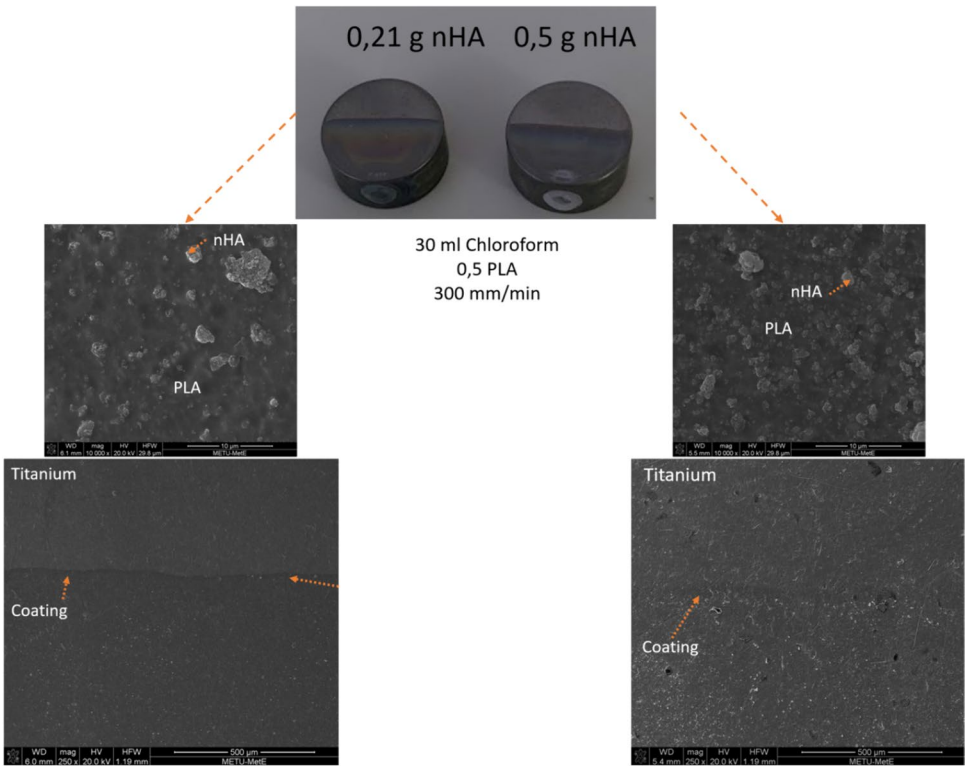

Fig. 6 SEM images of PLA:nHA composite coatings produced in 0.21 g (70:30) and 0.50 g (50:50) amounts of nHA

were 400 nm and 5 µm, respectively. A low accumulation of the coating was observed with no cracks although they applied five dip coating repetitions. Cracks, in contrast to that study, formed in the one-time dipping procedure in our study. The reason for this might be the properties of nHA that was used in our study. The rationale behind choosing nHA over HA is its superior capability to penetrate the micron-level pores of the gyroid discs. Another study [34], on the other hand, demonstrated that nHA is prone to accumulation and can cause some crack formation on the surfaces. The outcomes of that study supported the nHA application in our study.

Effects of Withdrawal Speed and Viscosity The coating process was carried out initially using a composite of 70:30 PLA:nHA prepared with 30 ml of chloroform. Withdrawal speeds of 300, 500, 750 and 1000 mm/min were tested as shown in Fig. 7(a). Pore clogging was observed during this stage; however, it showed a decreasing trend with increasing withdrawal speeds. Viscosity ratio was re-adjusted by increasing the chloroform volume to 50 ml to overcome this problem. The new solution composition of 70:30 was then used for the coating at the same withdrawal speed. Interpore clogging was not observed indicating that the clogging issue was resolved by increasing the withdrawal speed as exhibited in Fig. 7(b). The results were compatible with that of the literature [1, 5], which stated that a thicker coating layer consists of higher viscosity. The coating was evenly distributed inside the pores as shown in Fig. 8(b). PLA exhibited a uniform adhesion to the surface at a withdrawal speed of 300 mm/min. PLA however became fibrous and adhered less effectively to the surfaces in the 30 ml and 50 ml solutions as the withdrawal speed increased. Despite this, the coating managed to penetrate into each part of the disc and achieved

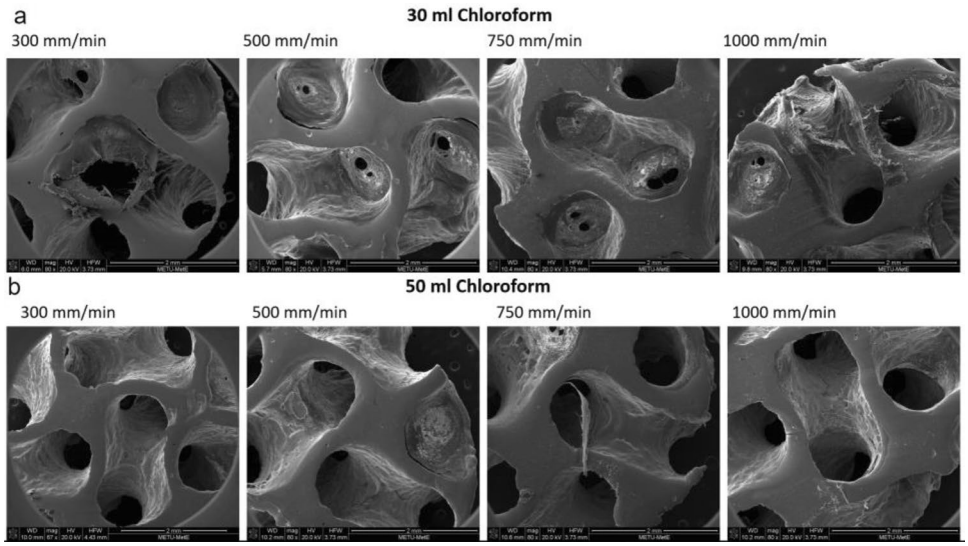

Fig. 7 **a** Gyroid SEM images of the dip coating made with PLA:nHA prepared composite in 30 ml chloroform from 300 mm/min to 1000 mm/min draw speed, (**b**) With PLA:nHA prepared composite in 50 ml chloroform at 300 mm/min Gyroid SEM images of dip coating up to 1000 mm/min drawing speed

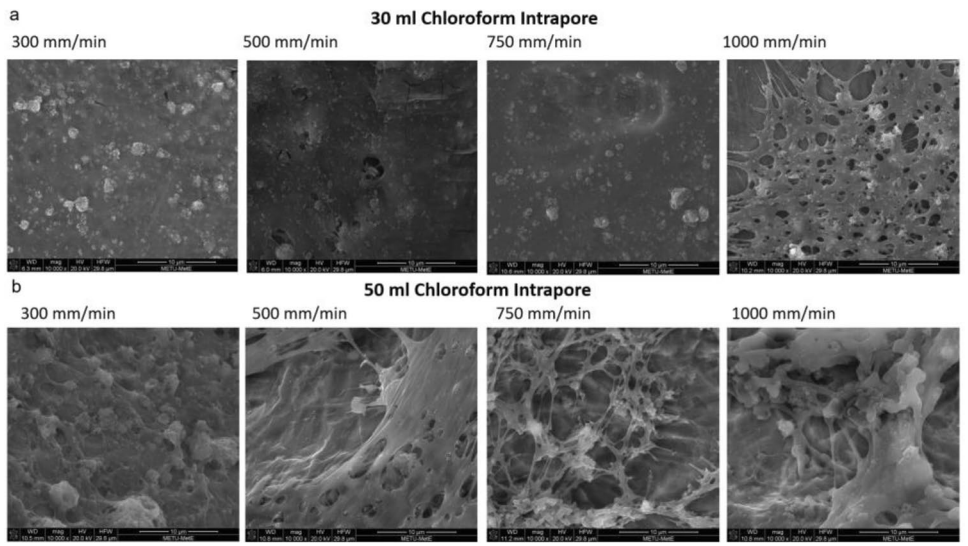

Fig. 8 **a** Intrapore SEM images of the dip coating made with 30 ml of PLA:nHA prepared composite in chloroform from 300 mm/min to 1000 mm/min draw speed, (**b**) 300 mm/min with PLA:nHA prepared composite in 50 ml chloroform intrapore SEM images of dip coating made from tensile to 1000 mm/min

the desired pore opening at a withdrawal speed of 1000 mm/min.

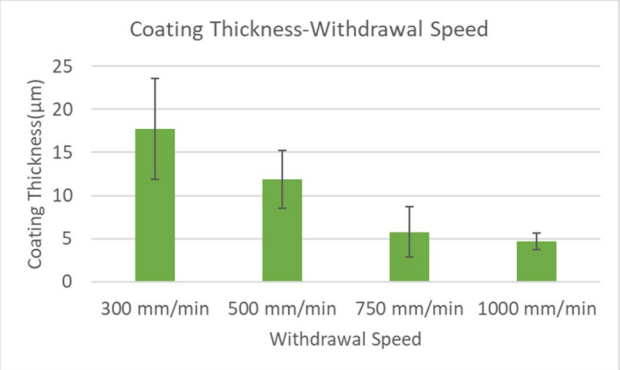

Fig. 9 Coating thicknesses of 50 ml chloroform 70:30 PLA:nHA composite coated solid titanium discs at 300, 500, 750 and 1000 mm/min drawing speeds

Coating thickness The coating thickness may differ at the edges of the Cp-Ti discs when the samples were coated. A previous study [35] reported that higher withdrawal speed created a thicker coating layer due to less drainage and lower evaporation. Our study however, revealed different results as shown in Fig. 9. Measurements illustrated that the coating thickness reduced as the withdrawal speed increased. At a withdrawal speed of 300 mm/min, the thickness was approximately 1.8 µm, while it decreased to 400 nm at a withdrawal speed of 1000 mm/min. A study [36] stated that 50–400 nm thick crack-free coatings can be obtained by accurately controlling the withdrawal speed. This range provided sufficient interconnectivity for the cell migration and nutrient transition without pore occlusion. Another study [16] also reached 400 nm coating thickness with dip coating of PLA:HA on titanium. Consequently, the optimized sol–gel composite solution of 70:30 PLA:nHA in 50 ml of chloroform proved to be suitable with the literature for porous discs when employing a withdrawal speed of 1000 mm/min. EDS analysis was furthermore conducted on solid Ti6Al4V discs

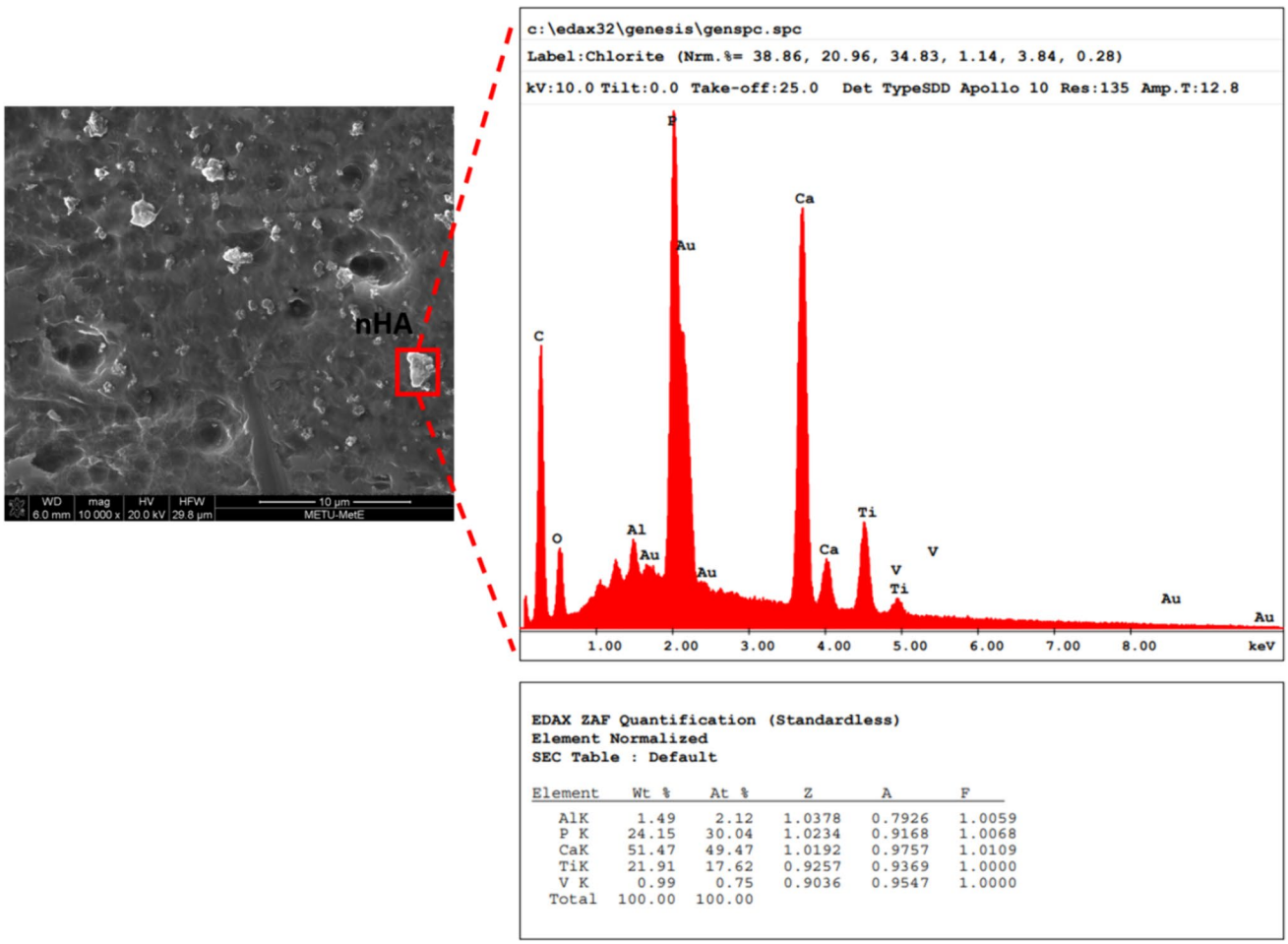

Fig. 10 SEM–EDS analysis of 50 ml chloroform 70:30 PLA:nHA composite coating on Ti6Al4V disc made at 1000 mm/min withdrawal speed

at a withdrawal speed of 1000 mm/min, which revealed the presence of a PLA:nHA composite coating on the surface of gyroid Cp-Ti discs. The analysis indicated that the presence of C and O elements correspond to the PLA while Ca and P elements meant nHA and shown in Fig. 10.

Silk fibroin composite coating 2% and 5% SF coatings were successfully applied to gyroid Cp-Ti discs as shown in Fig. 11. Thin and uniform silk layers contouring well to the topography of the gyroid Cp-Ti were noted by fluorescence microscopy. The coating material was detected on the pore surfaces as well as in the inner regions of the disc without interpore clogging. SF layers overlapped and accumulated thickly on the coating surface and open pore structures were maintained in the coating itself as exhibited in Fig. 12. Interconnectivities between adjacent pores were also noted. Bead-like SF formations and fixative fibrils were furthermore observed inside of the coating. The study [37] stated that silk fibroin coating on unsmooth titanium surfaces via the deposition method provides high stability through conductivity of titanium. The findings of silk fibroin deposition on gyroid Cp-Ti discs in our study are in line with the literature.

We furthermore analyzed the coating thickness of SF using SEM imaging of the cross-sectional area as shown in Fig. 13(a) and (b). The coating thickness was directly related to the SF concentrations. Wherein, 2% SF coating has an average thickness of 23.8 ± 3.3 µm while 5% SF deposit on the Cp-Ti surface corresponds to an average of 49.4 ± 2.9 µm thickness. The SF coating weight gave proportional results in Fig. 13(c). The coating with 5% SF solution was heavier than that of the 2% SF during the weight measurements. Significantly thicker coatings were obtained for the 5% SF concentration coating compared to the 2% concentration group ($p < 0.05$).

3.3 Biocompatibility tests results and discussions

Cytotoxicity analysis by MTT All groups, except the positive control group, presented higher absorbance values in the MTT cytotoxicity tests at 12, 24 and 48 h as shown in

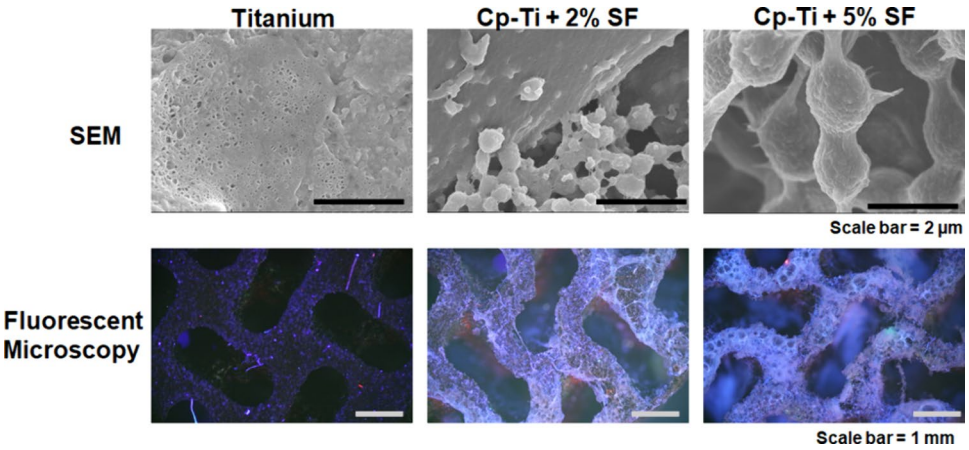

Fig. 11 Images of uncoated, 2% and 5% SF coated gyroid Cp-Ti discs under scanning electron microscopy and fluorescence microscope

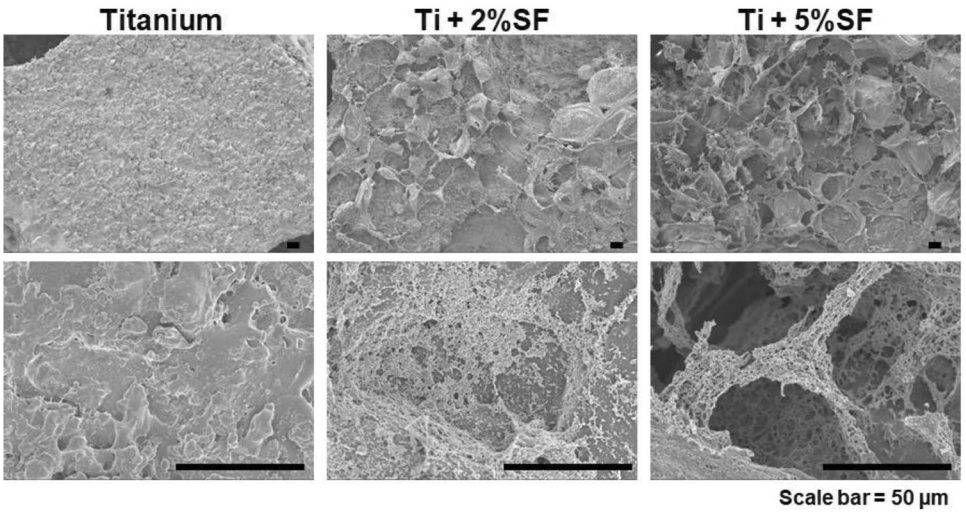

Fig. 12 SEM images showing thick deposition of SF coating with overlapping sheets, open porosity, formation of beads and anchoring fibrils which are the characteristics of SF. Scale bar = 50 µm

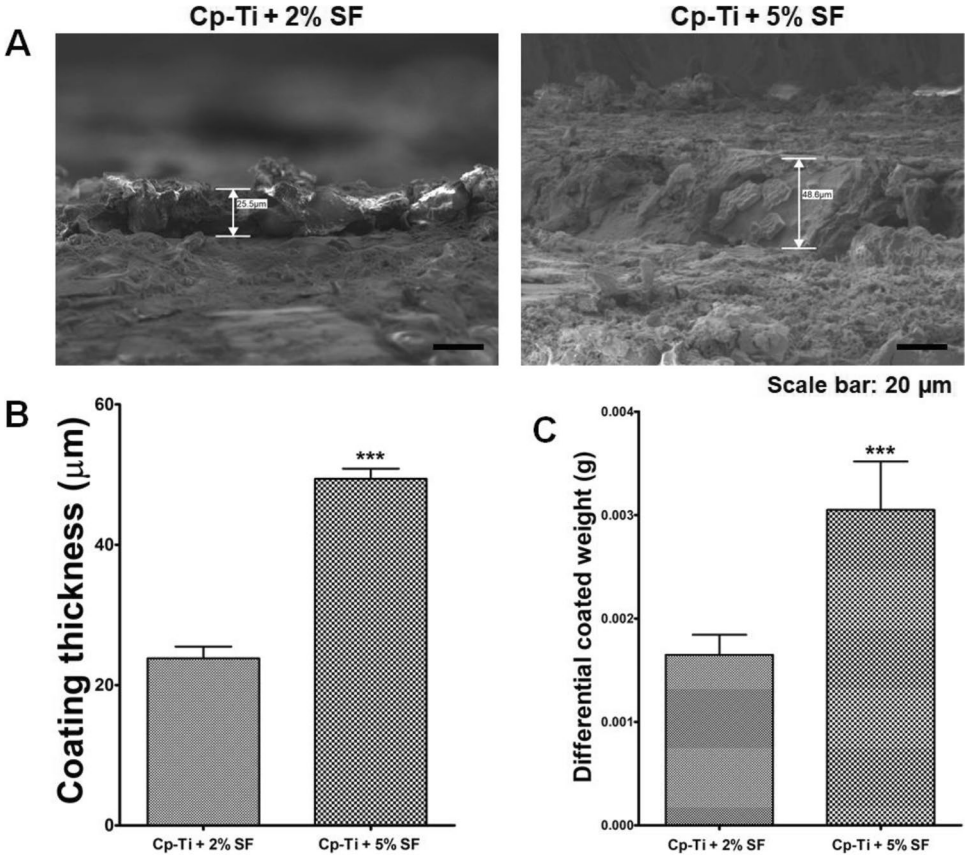

Fig. 13 Analyses of SF amount deposited on Cp-Ti surfaces. (**a**) Representative SEM micrograph measuring the coating thickness of SF-coated Cp-Ti. (**b**) Comparative graph of SF-coated Ti, showing the coating thickness. (**c**) Coating weight graph of 2% and 5% concentration SF solutions. $***P < 0.0001$

Fig. 14. Cell viability rates of them were calculated to be approximately 100% at 12 h. The negative control group, on the other hand showed higher cell viability at 24 and 48 h compared to the 12 h time variable, while the viability rates of the 24 and 48 h observations decreased in the other groups. Polyethylene application increased cell viability and created a significant difference compared to the positive control group at 24 h ($p = 0{,}024$). The reason for the higher absorbance in the negative control group compared to that of the Cp-Ti groups was due to higher cell proliferation. The coating surfaces of Cp-Ti exhibited a biocompatible behavior throughout the examination time periods. Another study [38] also indicated that the L929 cell control group exhibited a greater cell viability rate than polymer/HA-coated solid titanium plates in MTT analysis. Results of our study was in line with that study. Increased cell viability rate in coated Ti samples [38] nn the other hand was observed from one to seven days. Another study [39] stated that L929 cell viability in coated Ti samples was the highest on day 3 and then decreased on day 5. This finding supported the idea that cell proliferation was faster in the control group compared to coated Ti.

Cell viability analysis by live and dead cell assay The surface-adherent spindle shaped HDF were examined on the disc surfaces from day one to seven. Viable cells (green–blue) accumulated mostly at the edges of the thin walls. All groups exhibited lower healthy cell attachment between days one and three as shown in Fig. 15. The healthy cell volume increased from day five to seven in all groups. Red-blue labeled dead cells decreased in time due to the removal of the non-adherent cells at washing steps. Another study [40] specified that HA addition to Ti did not contribute to cell growth during the first few days, however significant increase in cell viability at all groups was observed at the end of the first week. Another study [41] indicated that cell adhesion was observed after day one and the cells generated a bridge between the pores from days three to seven. One other study [42] presented that cell metabolic activity and proliferation increased until day 7 in the porous of Ti6Al4V samples. Current literature confirms that cell viability rises on titanium surfaces in 7 days.

The 50:50 PLA:nHA coated sample exhibited higher cell attachment when compared to the 70:30 PLA:nHA coated and uncoated samples on day seven while the 70:30 PLA:nHA samples showed a minimum viability rate as shown in Fig. 16. The reason for fluctuations in viability rates might be the movement and attachment of the cells toward the pores. Our findings were in line with a former study [43]. Another study [44] presented that the cells

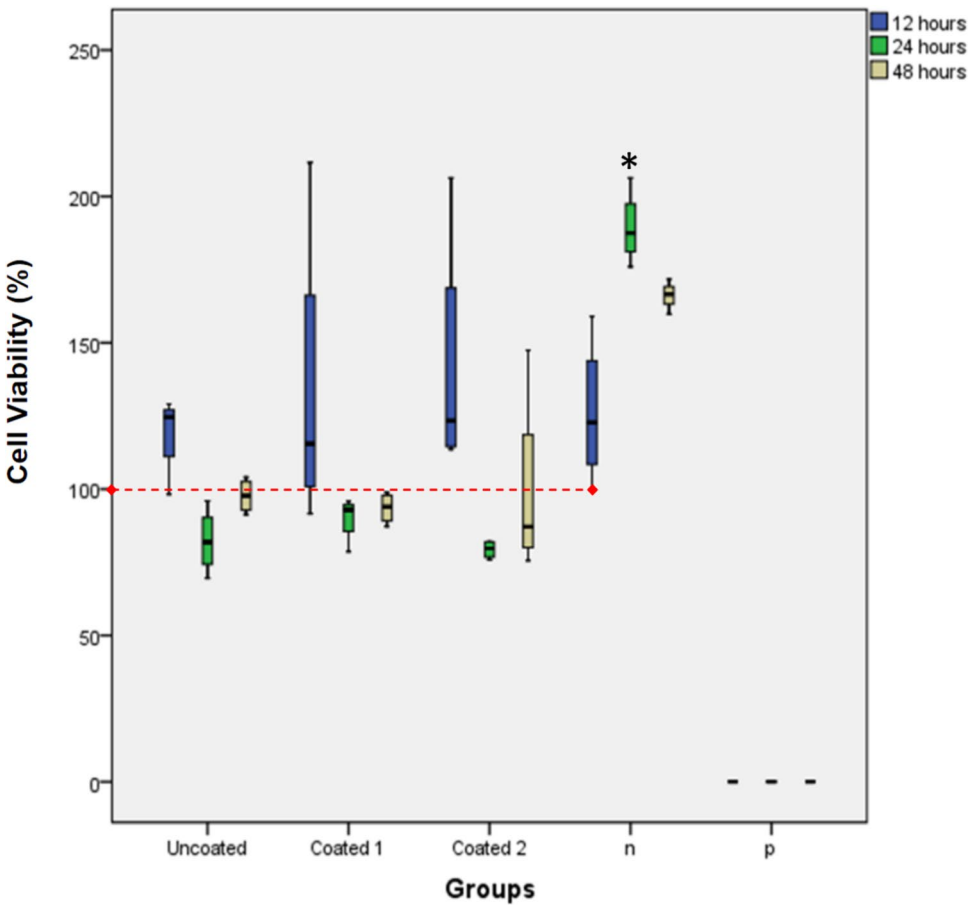

Fig. 14 The minimum, maximum and median absorbance values of the experimental and control groups at 12, 24 and 48 h. Coated 1 (70:30 PLA:nHA), Coated 2 (50:50 PLA:nHA), n (Polyethylene) and p (Latex) groups. Red line-the lowest value of the negative control group was taken as a reference for the 100% viability rate. (*) Significant difference from the positive control group for the 12 h ($P < 0.05$)

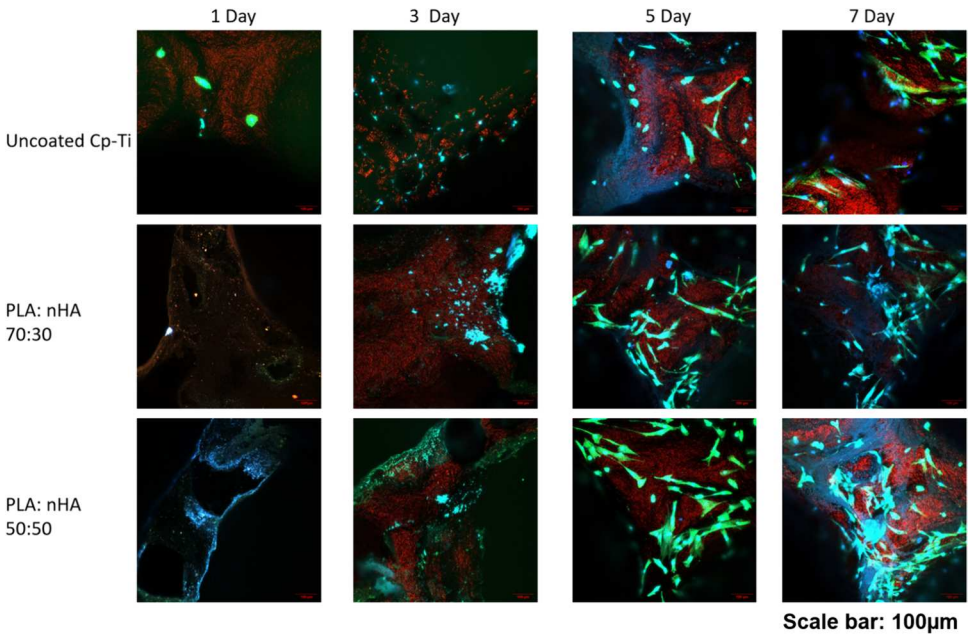

Fig. 15 Confocal images of HDF cells seeded on PLA:nHA coated and uncoated Cp-Ti discs

behaved in non-contact with thin walls. Imaging under higher magnification presented that the cells adhered semi-smoothly on to the Ti surfaces into the pores. One other study [45] showed that the cells are prone to progress into the pores. The volume of healthy cells increased as the incubation time increased in the coated groups (50:50).

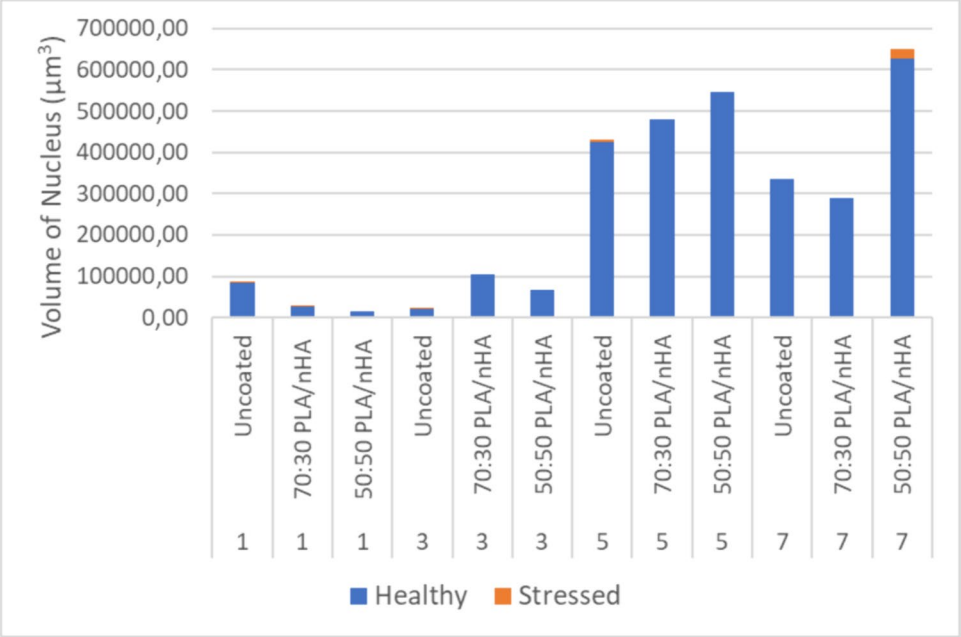

Fig. 16 Total volume of the nucleus of PLA:nHA coated and uncoated groups

Increasing the amount of HA might be the reason for this increase. Another study [46] also proved that increasing the HA rate had a positive effect on cell proliferation on the polymer and polymer/HA composite surfaces. One other study [47] also compared nano and micro HA coated on cp-Ti. Superior cell proliferation at micro-HA against nano-HA was shown during seven days. Cell performance on nano HA however increased on day 14. The literature supports that HA coating promotes cell viability in titanium discs also, using nano HA led to increased cell metabolic activity in the longer term.

Confocal microscopy images were enhanced with fluorescence microscopy as shown in Fig. 17. Increasing proliferation rates after day three was observed in all groups including the control group.

SEM images clarified HDF cell's attachment on material surfaces as shown in Fig. 18 on day seven. Cell–cell and cell-titanium disc interactions were identified. These cells synthesized the extracellular matrix (ECM). The structure of the ECM was better visualized in SEM analysis unlike confocal microscopy. The network formed because of interactions in the ECM with the cell's specific spindle shape was observed to cover the cells.

HDF cells with different concentrations of silk fibroin coating on Cp-Ti were cultured for seven days to evaluate cell viability and proliferation on the coated Cp-Ti discs as

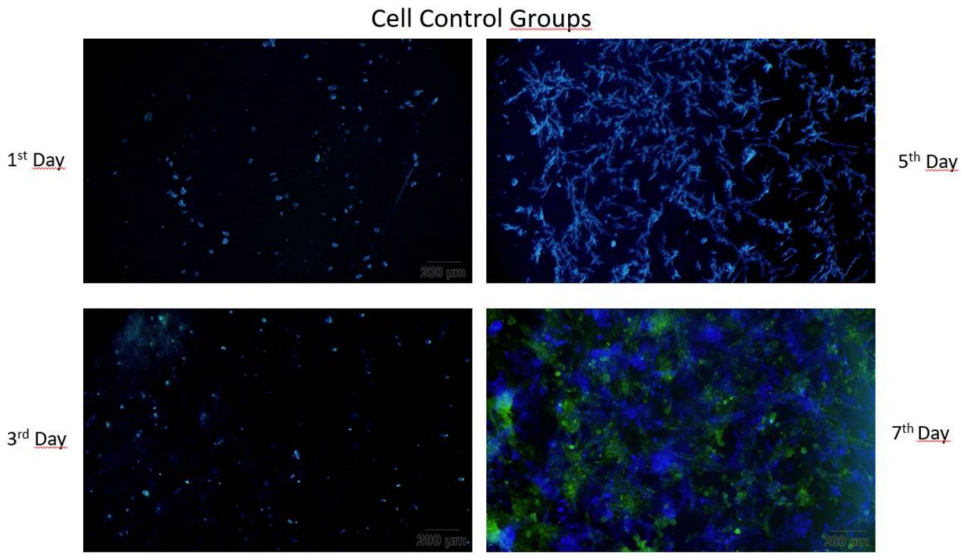

Fig. 17 Representative fluorescence images of cells on days 1, 3, 5 and 7

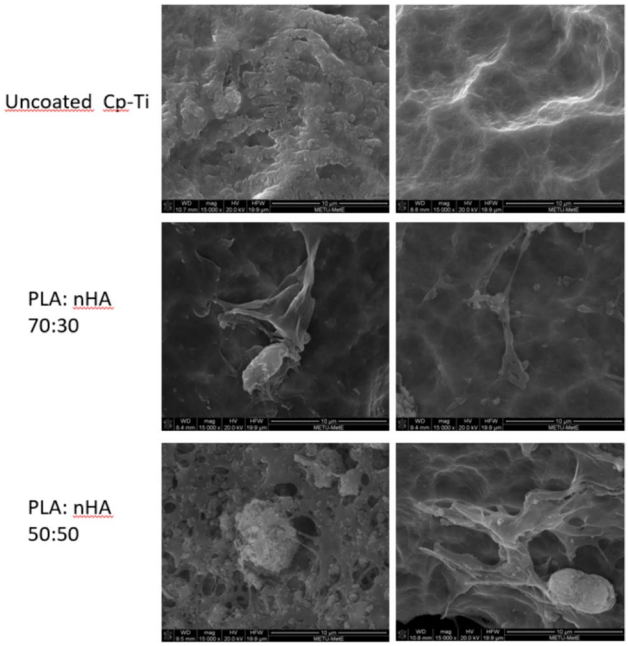

Fig. 18 SEM images of PLA:nHA composite coating on the 7th day

shown in Fig. 19. The number of viable cells was higher in the coated groups. A gradual increase in HDF viability according to the culture time with the change in cell morphology was observed in all groups. In particular, the 5% silk fibroin-coated group showed the highest cell proliferation and the least dead cell numbers. These results show the optimal concentration of silk fibroin coating on Cp-Ti, indicating a suitable environment for cell viability and minimal cytotoxicity while avoiding interpore clogging The study [48] specified that silk fibroin coating provides high cell activity and osseointegration.

A limitation of this study was that a statistical evaluation for the cell viability analysis by live and dead cell assay could not be performed. We used image analysis in only one sample per group, however this limitation was overcome by including volume analysis of cell nucleus using a software. The region filtered volumes of cell nucleus were calculated separately for both healthy and stressed cells as shown in Fig. 16. The PI dye however attached to the surface of the material in addition to the stressed cell nucleus. Red fluorescent regions were therefore ignored during analysis with the 3D Tool Kit. Time-laps imaging for observing the time dependent changes on the surfaces of the coating is planned to be used in future studies.

Another limitation of the study was that long-term coating stability characterizations were not undertaken. Although cracks and delamination were not observed on the coating surface during SEM and EDS characterizations, the importance of long-term coating stability under physiological conditions in the human body cannot be denied [49, 50]. Electrochemical impedance spectroscopy quantifies impedance change to provide insight into coating stability [51]. Degradation methods are immersion tests with simulated body fluids [52, 53] and accelerated aging tests with temperature and humidity, which can be considered to measure corrosion resistance [54]. Mechanical test methods include scratch tests [55] as well as histological analysis in-vitro studies with

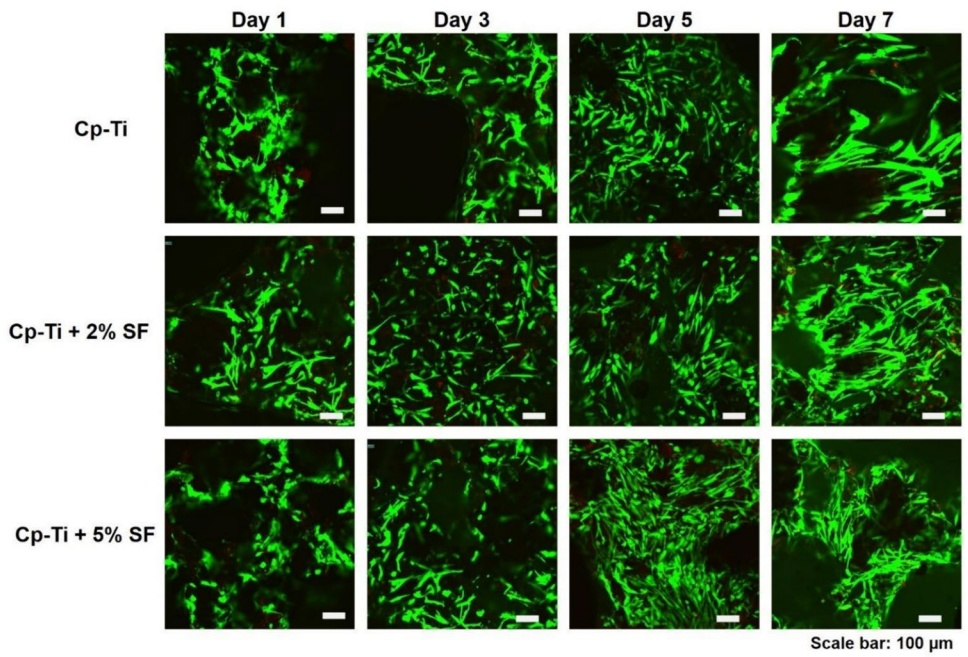

Fig. 19 Representative live and dead images of different concentrations of silk fibroin coated Cp-Ti samples

animal experiments to understand coating stability performance over time [56]. Such studies can be planned for future studies.

4 Conclusion

Achieving bone-mimicking gyroid structures using additive manufacturing and an ideal coating for biocompatibility was examined in this study. A cleaning process was first developed to remove the non-melted particles adhering to the surface of the gyroid Cp-Ti. A minute of acid-etching enabled homogeneous micro-pit distribution and supported the coating stability on the surface. Lack of surface roughness measurement was the limitation of this study however obtaining a smoother surface could have decreased cell attachments.

Two different coating materials and coating methods were utilized after the cleaning process. These coating and biological processes were completed in separate experimental conditions. The success criteria for the coating were the obtainment of crack-free and homogeneous surfaces with 400 nm coating thickness by adjusting the accumulation, withdrawal speed and viscosity factors in a controlled manner in the dip coating method. The coatings of PLA:nHA and silk fibroin materials on gyroid Cp-Ti discs were achieved without interpore clogging. The adjusted coating contributed positively to the functionality of the implant in in-vitro experiments. The confocal images presented higher cell proliferation on the coating surfaces. PLA:nHA (30% to 50%) and silk-fibroin (2% to 5%) contributed to greater cell adhesion, also leading to accelerated cell proliferation. Biocompatibility characterizations of both optimized coatings showed the stability of the coatings on titanium surfaces in the 7 days. However, in-vivo animal experiments are needed in future studies for long-term stability assessments. Electrochemical and degradation tests will also ensure valuable data for stability performance.

Acknowledgements The project entitled Development of a Selective Laser Melting (SLM) Technology Platform for the Production and Characterization of Calcium Phosphate/PLGA Composite Coated Porous Titanium Mini Plates for Maxillofacial, Hand and Ear-Nose-Throat (ENT) Surgery (PorouSLM) was funded by the Cooperation of The Scientific and Technological Research Council of Turkey (TUBITAK) and the National Research Foundation (NRF) of Korea under grant agreement TUBITAK No 120N943 and NRF No 2020K2A9A1A0610851. Part of this study was presented at the 31st Annual Meeting of the European Orthopaedic Research Society (EORS2023) between 27 and 29 September 2023 in Porto, Portugal (Abstract Book pp: 221). Feza Korkusuz MD is an active member of the Turkish Academy of Sciences (TÜBA).

Funding Open access funding provided by the Scientific and Technological Research Council of Türkiye (TÜBİTAK).

Data Availability All data is presented in the figures, graphics and tables in the context of the manuscript.

References

1. F.M. Chen, X. Liu, Advancing biomaterials of human origin for tissue engineering. /pmc/articles/PMC4808059/?report=abstract (2016)
2. Z. AA, Additively manufactured porous metallic biomaterials. J. Mater. Chem. B. **7**, 4088–4117 (2019). https://doi.org/10.1039/C9TB00420C
3. F.N. Depboylu, E. Yasa, Ö. Poyraz, J. Minguella-Canela, F. Korkusuz, M.A. De los Santos López, Titanium based bone implants production using laser powder bed fusion technology. J. Mater. Res. Technol. **17**, 1408–1426 (2022). https://doi.org/10.1016/J.JMRT.2022.01.087
4. F.N. Depboylu, E. Yasa, O. Poyraz, F. Korkusuz, Thin-walled commercially pure titanium structures: laser powder bed fusion process parameter optimization. Mach. **11**, 272 (2023). https://doi.org/10.3390/MACHINES11020272
5. J. Shi, L. Zhu, L. Li, Z. Li, J. Yang, X. Wang, A TPMS-based method for modeling porous scaffolds for bionic bone tissue engineering. Sci. Rep. **8**(1), 1–10 (2018). https://doi.org/10.1038/s41598-018-25750-9
6. S. Vijayavenkataraman, L. Zhang, S. Zhang, J.Y.H. Fuh, W.F. Lu, Triply periodic minimal surfaces sheet scaffolds for tissue engineering applications: An optimization approach toward biomimetic scaffold design. ACS Appl. Bio Mater. **1**, 259–269 (2018). https://doi.org/10.1021/ACSABM.8B00052/ASSET/IMAGES/MEDIUM/MT-2018-000523_0008.GIF
7. D. Wang, G. He, Y. Tian, N. Ren, W. Liu, X. Zhang, Dual effects of acid etching on cell responses and mechanical properties of porous titanium with controllable open-porous structure. J. Biomed. Mater. Res. B Appl. Biomater. **108**, 2386–2395 (2020). https://doi.org/10.1002/JBM.B.34571
8. G. Pyka, A. Burakowski, G. Kerckhofs, M. Moesen, S. Van Bael, J. Schrooten, M. Wevers, Surface modification of Ti6Al4V open porous structures produced by additive manufacturing. Adv. Eng. Mater. **14**, 363–370 (2012). https://doi.org/10.1002/adem.201100344
9. J.E. González, G. de Armas, J. Negrin, A.M. Beltrán, P. Trueba, F.J. Gotor, E. Peón, Y. Torres, Influence of successive chemical and thermochemical treatments on surface features of Ti6Al4V samples manufactured by SLM. Met. **11**, 313 (2021). https://doi.org/10.3390/MET11020313
10. E. Pehlivan, J. Džugan, J. Fojt, R. Sedláček, S. Rzepa, M. Daniel, Post-processing treatment impact on mechanical properties of SLM deposited Ti-6Al-4 V porous structure for biomedical application. Materials (Basel). **13**, 5167 (2020). https://doi.org/10.3390/ma13225167
11. B. Wysocki, J. Idaszek, K. Szlazak, K. Strzelczyk, T. Brynk, K.J. Kurzydłowski, W. Świeszkowski, Post processing and biological evaluation of the titanium scaffolds for bone tissue

engineering. Materials (Basel). **9**, 197 (2016). https://doi.org/10.3390/ma9030197
12. E. Zhang, Y. Wang, F. Gao, S. Wei, Y. Zheng, Enhanced bioactivity of sandblasted and acid-etched titanium surfaces. Adv. Mater. Res. **79–82**, 393–396 (2009). https://doi.org/10.4028/WWW.SCIENTIFIC.NET/AMR.79-82.393
13. M.A. Surmeneva, D. Khrapov, K. Prosolov, M. Kozadayeva, A. Koptyug, A. Volkova, A. Paveleva, R.A. Surmenev, The influence of chemical etching on porous structure and mechanical properties of the Ti6AL4V Functionally Graded Porous Scaffolds fabricated by EBM. Mater. Chem. Phys. **275**, 125217 (2022). https://doi.org/10.1016/J.MATCHEMPHYS.2021.125217
14. N. Balaban, TİTANYUM VE ALAŞIMLARININ BİYOUYUMLULUKLARININ İNCELENMESİ. (2007). https://polen.itu.edu.tr/handle/11527/9296. Accessed Jun 2023
15. S.C. Lee, K.A. Jung, C.H. Nam, T.H. Kim, N.K. Ahn, S.H. Hwang, Acetabular screw head-induced ceramic acetabular liner fracture in cementless ceramic-on-ceramic total hip arthroplasty. Orthopedics **33**, 353–353 (2010). https://doi.org/10.3928/01477447-20100329-30
16. I.K. Soylu, University of Technology Sydney (Australia) ProQuest Dissertations & Theses. 30722244 (2020). https://www.proquest.com/docview/2890698251?pq-origsite=gscholar&fromopenview=true&sourcetype=Dissertations%20&%20Theses
17. M.F. Mohd Yusoff, M.R. Abdul Kadir, N. Iqbal, M.A. Hassan, R. Hussain, Dipcoating of poly (ε-caprolactone)/hydroxyapatite composite coating on Ti6Al4V for enhanced corrosion protection. Surf. Coatings Technol. **245**, 102–107 (2014). https://doi.org/10.1016/J.SURFCOAT.2014.02.048
18. O.A. Hamed, M.E. Khan, A.U. Khan, G. Rabbani, M.S. Alomar, A.H. Bashiri, W. Zakri, Adherence and activation of human mesenchymal stromal cells on brushite coated porous titanium. Results Eng. **19**, 101245 (2023). https://doi.org/10.1016/J.RINENG.2023.101245
19. H. Shao, Q. Zhang, M. Sun, M. Wu, X. Sun, Q. Wang, S. Tong, Effects of hydroxyapatite-coated porous titanium scaffolds functionalized by exosomes on the regeneration and repair of irregular bone. Front. Bioeng. Biotechnol. **11**, 1283811 (2023). https://doi.org/10.3389/FBIOE.2023.1283811/BIBTEX
20. J. Xu, D. Wu, B. Ge, M. Li, H. Yu, F. Cao, W. Wang, Q. Zhang, P. Yi, H. Wang, L. Song, L. Liu, J. Li, D. Zhao, Selective laser melting of the porous Ta scaffold with Mg-doped calcium phosphate coating for orthopedic applications. ACS Biomater. Sci. Eng.Biomater. Sci. Eng. **10**, 1435–1447 (2024). https://doi.org/10.1021/ACSBIOMATERIALS.3C01503/ASSET/IMAGES/MEDIUM/AB3C01503_0009.GIF
21. J. Lock, T.Y. Nguyen, H. Liu, Nanophase hydroxyapatite and poly(lactide-co-glycolide) composites promote human mesenchymal stem cell adhesion and osteogenic differentiation in vitro. J. Mater. Sci. Mater. Med. **23**, 2543–2552 (2012). https://doi.org/10.1007/s10856-012-4709-0
22. H. Najafi, A. Nemati, Z. Sadeghian, Crystallisation kinetics of hydroxyapatite thin films prepared by sol-gel process. Adv. Appl. Ceram. **109**, 313–317 (2010). https://doi.org/10.1179/174367609X422144
23. H.R. Bakhsheshi-Rad, E. Hamzah, C.P. Shuang, F. Berto, Preparation of poly(ε-caprolactone)-hydroxyapatite composite coating for improvement of corrosion performance of biodegradable magnesium. Mater. Des. Process. Commun. **2**, e170 (2020). https://doi.org/10.1002/MDP2.170
24. M. Hrubovčáková, M. Kupková, M. Džupon, M. Giretová, Ľ. Medvecký, R. Džunda, Electrochemical science biodegradable polylactic acid and polylactic acid/hydroxyapatite coated iron foams for bone replacement materials. Int. J. Electrochem. Sci.Electrochem. Sci. **12**, 11122–11136 (2017). https://doi.org/10.20964/2017.12.53
25. R. Elia, C.D. Michelson, A.L. Perera, M. Harsono, G.G. Leisk, G. Kugel, D.L. Kaplan, Silk electrogel coatings for titanium dental implants. 10.1177/0885328214561536 **29**, 1247–1255 (2014). https://doi.org/10.1177/0885328214561536
26. D. Maniglio, W. Bonani, G. Bortoluzzi, E. Servoli, A. Motta, C. Migliaresi, Electrodeposition of silk fibroin on metal substrates. 10.1177/0883911510374384. **25**, 441–454 (2010). https://doi.org/10.1177/0883911510374384
27. Z. Zhang, Y. Qu, X. Li, S. Zhang, Q. Wei, Y. Shi, L. Chen, Electrophoretic deposition of tetracycline modified silk fibroin coatings for functionalization of titanium surfaces. Appl. Surf. Sci. **303**, 255–262 (2014). https://doi.org/10.1016/J.APSUSC.2014.02.160
28. S.H. Kim, Y.K. Yeon, J.M. Lee, J.R. Chao, Y.J. Lee, Y.B. Seo, M.T. Sultan, O.J. Lee, J.S. Lee, S.I.I. Yoon, I.S. Hong, G. Khang, S.J. Lee, J.J. Yoo, C.H. Park, Precisely printable and biocompatible silk fibroin bioink for digital light processing 3D printing. Nat. Commun.Commun. **9**, 1–14 (2018). https://doi.org/10.1038/s41467-018-03759-y
29. A.H. Choi, B. Ben-Nissan, Calcium phosphate nanocomposites for biomedical and dental applications: Recent developments. In: Handbook of composites from renewable materials. pp. 423–450. Wiley (2017)
30. F.N. Depboylu, Kaplanmış Gözenekli Ti6Al4V İmplantların Lazer Metal Toz Ergitme (LAM) Teknolojisi ile Üretimi ve Karakterizasyonu. (2023). https://openaccess.hacettepe.edu.tr/xmlui/handle/11655/33292. Accessed Jun 2023
31. eos, Material data sheet-FlexLine EOS Titanium TiCP grade 2. (2022)
32. S.H. Kim, H. Hong, O. Ajiteru, M.T. Sultan, Y.J. Lee, J.S. Lee, O.J. Lee, H. Lee, H.S. Park, K.Y. Choi, J.S. Lee, H.W. Ju, I.S. Hong, C.H. Park, 3D bioprinted silk fibroin hydrogels for tissue engineering. Nat. Protoc. **16**, 5484–5532 (2021). https://doi.org/10.1038/S41596-021-00622-1
33. X.L. Yang, X.F. Du, Z.L. Xu, Z.S. Liang, L.L. Xiong, Progress in processing of porous titanium: a review. Rare Met. **43**(5), 1932–1955 (2024). https://doi.org/10.1007/S12598-023-02570-Z
34. V.M. Suntharavel Muthaiah, M. Rajput, A. Tripathi, S. Suwas, K. Chatterjee, Electrophoretic deposition of nanocrystalline calciumphosphate coating for augmenting bioactivity of additively manufactured Ti-6Al-4V. ACS Mater. Au. **2**, 132 (2022). https://doi.org/10.1021/ACSMATERIALSAU.1C00043
35. W.Y. Maeng, J.H. Yoon, D.J. Kim, Effect of process conditions (withdrawal rate and coating repetition) on morphological characteristics of sol–gel TiO2 film during dip coating. J. Coatings Technol. Res. **17**, 1171–1193 (2020). https://doi.org/10.1007/S11998-020-00337-0/FIGURES/26
36. A.H. Choi, S. Cazalbou, B. Ben-Nissan, Nanobiomaterial coatings in dentistry. Front. Oral Biol.. Oral Biol. **17**, 49–61 (2015). https://doi.org/10.1159/000381693
37. A. Arkhangelskiy, D. Maniglio, A. Bucciarelli, V.K. Yadavalli, A. Quaranta, Plasma-assisted deposition of silk fibroin on different surfaces. Adv. Mater. Interfaces **8**, 2100324 (2021). https://doi.org/10.1002/ADMI.202100324
38. W. Diwu, X. Dong, O. Nasif, S.A. Alharbi, J. Zhao, W. Li, In-vivo investigations of hydroxyapatite/Co-polymeric composites coated titanium plate for bone regeneration. Front. Cell Dev. Biol. **8**, (2021). https://doi.org/10.3389/FCELL.2020.631107
39. Y.D. Nokoorani, A. Shamloo, M. Bahadoran, H. Moravvej, Fabrication and characterization of scaffolds containing different amounts of allantoin for skin tissue engineering. Sci. Rep. **11**(1), 1–20 (2021). https://doi.org/10.1038/s41598-021-95763-4
40. M. Shbeh, Z.J. Wally, M. Elbadawi, M. Mosalagae, H. Al-Alak, G.C. Reilly, R. Goodall, Incorporation of HA into porous titanium to form Ti-HA biocomposite foams. J. Mech. Behav. Biomed. Mater. **96**, 193–203 (2019). https://doi.org/10.1016/J.JMBBM.2019.04.043

41. J. Qu, X. Lu, D. Li, Y. Ding, Y. Leng, J. Weng, S. Qu, B. Feng, F. Watari, Silver/hydroxyapatite composite coatings on porous titanium surfaces by sol-gel method. J. Biomed. Mater. Res. Part B Appl. Biomater. 97B, 40–48 (2011). https://doi.org/10.1002/JBM.B.31784
42. C. Wang, D. Xu, S. Li, C. Yi, X. Zhang, Y. He, D. Yu, Effect of pore size on the physicochemical properties and osteogenesis of Ti6Al4V porous scaffolds with bionic structure. ACS Omega **5**, 28684–28692 (2020). https://doi.org/10.1021/ACSOMEGA.0C03824/ASSET/IMAGES/LARGE/AO0C03824_0012.JPEG
43. R. Costa-Almeida, M. Gomez-Lazaro, C. Ramalho, P.L. Granja, R. Soares, S.G. Guerreiro, Fibroblast-endothelial partners for vascularization strategies in tissue engineering. Tissue Eng. Part A **21**, 1055–1065 (2015). https://doi.org/10.1089/TEN.TEA.2014.0443
44. T. Zhang, X. Zhang, M. Mao, J. Li, T. Wei, H. Sun, Chitosan/hydroxyapatite composite coatings on porous Ti6Al4V titanium implants: in vitro and in vivo studies. J. Periodontal Implant Sci. **50**, 392 (2020). https://doi.org/10.5051/JPIS.1905680284
45. X. Fu, X. Zhou, P. Liu, H. Chen, Z. Xiao, B. Yuan, X. Yang, X. Zhu, K. Zhang, X. Zhang, The optimized preparation of HA/L-TiO2/D-TiO2 composite coating on porous titanium and its effect on the behavior osteoblasts. Regen. Biomater. **7**, 505–514 (2020). https://doi.org/10.1093/RB/RBAA013
46. K.W. Lee, S. Wang, M.J. Yaszemski, L. Lu, Physical properties and cellular responses to crosslinkable poly(propylene fumarate)/hydroxyapatite nanocomposites. Biomaterials **29**, 2839–2848 (2008). https://doi.org/10.1016/J.BIOMATERIALS.2008.03.030
47. A.M. Vilardell, N. Cinca, N. Garcia-Giralt, S. Dosta, I.G. Cano, X. Nogués, J.M. Guilemany, Functionalized coatings by cold spray: An in vitro study of micro- and nanocrystalline hydroxyapatite compared to porous titanium. Mater. Sci. Eng. C **87**, 41–49 (2018). https://doi.org/10.1016/J.MSEC.2018.02.009
48. S. Popescu, M.E. Zarif, C. Dumitriu, C. Ungureanu, C. Pirvu, Silk fibroin-based hybrid nanostructured coatings for titanium implantable surfaces modification. Coatings **10**, 518 (2020). https://doi.org/10.3390/COATINGS10060518
49. J. Sánchez-Bodón, J.A. Del Olmo, J.M. Alonso, I. Moreno-Benítez, J.L. Vilas-Vilela, L. Pérez-Álvarez, Bioactive coatings on titanium: a review on hydroxylation, Self-Assembled Monolayers (SAMs) and surface modification strategies. Polymers (Basel). **14**, 165 (2022). https://doi.org/10.3390/POLYM14010165
50. X. Chen, J. Zhou, Y. Qian, L.Z. Zhao, Antibacterial coatings on orthopedic implants. Mater. Today Bio. **19**, 100586 (2023). https://doi.org/10.1016/J.MTBIO.2023.100586
51. H.T. Zaher, M.A. Hefnawy, S.S. Medany, S.M. Kamel, S.A. Fadlallah, Synergetic effect of essential oils and calcium phosphate nanoparticles for enhancement the corrosion resistance of titanium dental implant. Sci. Rep. **14**, (2024). https://doi.org/10.1038/S41598-024-52057-9
52. P. Peng, S. Kumar, N.H. Voelcker, E. Szili, R.S.C. Smart, H.J. Griesser, Thin calcium phosphate coatings on titanium by electrochemical deposition in modified simulated body fluid. J. Biomed. Mater. Res. Part A. **76A**, 347–355 (2006). https://doi.org/10.1002/JBM.A.30514
53. Y. Wang, S. Zhang, X. Zeng, K. Cheng, M. Qian, W. Weng, In vitro behavior of fluoridated hydroxyapatite coatings in organic-containing simulated body fluid. Mater. Sci. Eng. C. **27**, 244–250 (2007). https://doi.org/10.1016/J.MSEC.2006.03.012
54. C. Sanon, J. Chevalier, T. Douillard, R.J. Kohal, P.G. Coelho, J. Hjerppe, N.R.F.A. Silva, Low temperature degradation and reliability of one-piece ceramic oral implants with a porous surface. Dent. Mater. **29**, 389–397 (2013). https://doi.org/10.1016/J.DENTAL.2013.01.007
55. I. Karacan, B. Ben-Nissan, H.A. Wang, A. Juritza, M.V. Swain, W.H. Müller, J. Chou, A. Stamboulis, I.J. Macha, V. Taraschi, Mechanical testing of antimicrobial biocomposite coating on metallic medical implants as drug delivery system. Mater. Sci. Eng. C **104**, 109757 (2019). https://doi.org/10.1016/J.MSEC.2019.109757
56. H. Ao, J. Zong, Y. Nie, Y. Wan, X. Zheng, An in vivo study on the effect of coating stability on osteointegration performance of collagen/hyaluronic acid multilayer modified titanium implants. Bioact. Mater. **3**, 97 (2018). https://doi.org/10.1016/J.BIOACTMAT.2017.07.004